Journal of Theoretical Biology 567 (2023) 111490

Contents lists available at ScienceDirect

Journal of Theoretical Biology

journal homepage: www.elsevier.com/locate/yjtbi

HIV infection dynamics and viral rebound: Modeling results from humanized mice

Ting Guo [a], Qi Deng [b], Zhipeng Qiu [c], Libin Rong [d,*]

[a] Aliyun School of Big Data, Changzhou University, Changzhou, 213164, China
[b] School of Science, Nanjing University of Science and Technology, Nanjing 210094, China
[c] Center for Basic Teaching and Experiment, Nanjing University of Science and Technology, Jiangyin 214443, China
[d] Department of Mathematics, University of Florida, Gainesville, FL 32611, USA

ARTICLE INFO

Keywords:
Humanized mouse models
Mathematical models
Data fitting
Treatment interruption
Viral rebound

ABSTRACT

Despite years of combined antiretroviral therapy (cART), HIV persists in infected individuals. The virus also rebounds after the cessation of cART. The sources contributing to viral persistence and rebound are not fully understood. When viral rebound occurs, what affects the time to rebound and how to delay the rebound remain unclear. In this paper, we started with the data fitting of an HIV infection model to the viral load data in treated and untreated humanized myeloid-only mice (MoM) in which macrophages serve as the target of HIV infection. By fixing the parameter values for macrophages from the MoM fitting, we fit a mathematical model including the infection of two target cell populations to the viral load data from humanized bone marrow/liver/thymus (BLT) mice, in which both CD4+ T cells and macrophages are the target of HIV infection. Data fitting suggests that the viral load decay in BLT mice under treatment has three phases. The loss of infected CD4+ T cells and macrophages is a major contributor to the first two phases of viral decay, and the last phase may be due to the latent infection of CD4+ T cells. Numerical simulations using parameter estimates from the data fitting show that the pre-ART viral load and the latent reservoir size at treatment cessation can affect viral growth rate and predict the time to viral rebound. Model simulations further reveal that early and prolonged cART can delay the viral rebound after cessation of treatment, which may have implications in the search for functional control of HIV infection.

1. Introduction

Acquired immune deficiency syndrome (AIDS) is one of the leading causes of death in the world, especially in Sub-Saharan Africa. As the pathogenic agent of AIDS, HIV mainly infects activated CD4+ T cells (Aiamkitsumrit et al., 2015; Micci et al., 2014). In addition to CD4+ T cells, HIV also infects other cells, such as macrophages (Stevenson and Gendelman, 1994; Bol et al., 2009; Gorry et al., 2014; Sharova et al., 2005). CD4+ T cells and macrophages are important components of the immune system and play a critical role in defending against viral infection (Levy, 2001; Okoye and Picker, 2013). The progressive depletion of these cells has devastating effects on immune regulation, eventually resulting in the death of patients due to a series of opportunistic infections.

Different classes of antiretroviral drugs targeting specific stages of the HIV life cycle have been developed, including fusion inhibitors, reverse transcriptase inhibitors, integrase inhibitors, and protease inhibitors. The combined antiretroviral therapy (cART) containing three to five antiretroviral drugs has proven to be very effective in suppressing viral replication. It can reduce the plasma viral load to below the detection limit of standard assays, usually 50 RNA copies/ml. However, the current treatment cannot eliminate the virus and HIV persists in patients despite suppressive cART for a prolonged time (Collier et al., 1996; Palmer et al., 2008; Furtado et al., 1999; Maldarelli, 2011). The sources of viral persistence under cART are not fully understood. The latent reservoir, consisting of a small population of latently infected CD4+ T cells (Chun et al., 2003), is considered an important reason for the persistence of viremia (Richman et al., 2009; Barton et al., 2013; Katlama et al., 2013). These latent cells remain in the resting state under treatment (Wong et al., 1997) but can be activated and produce new virions, inducing viral rebound after the cessation of cART (Marsden et al., 2020).

There are two objectives for the management of HIV infection: a sterilizing cure that completely eradicates the virus and a functional cure that aims to control plasma HIV RNA to an undetectable or low

* Corresponding author.
E-mail address: libinrong@ufl.edu (L. Rong).

https://doi.org/10.1016/j.jtbi.2023.111490
Received 12 June 2022; Received in revised form 22 March 2023; Accepted 5 April 2023
Available online 11 April 2023
0022-5193/© 2023 Elsevier Ltd. All rights reserved.

level in the absence of antiretroviral treatment. Given the difficulty in eradicating HIV, a functional cure seems to be a more reachable short-term goal. Many efforts have been devoted to delaying viral rebound after therapy interruption in HIV-infected individuals (Hocqueloux et al., 2010; Sáez-Cirión et al., 2013; Wolfgang et al., 2013). In the VISCONTI study (Hocqueloux et al., 2010; Sáez-Cirión et al., 2013), patients received cART shortly after HIV exposure and some have the viral load controlled to undetectable levels for several years after the discontinuation of therapy. In another study (Wolfgang et al., 2013), 165 patients received cART within 6 months of seroconversion and achieved viral load < 400 RNA copies/ml at treatment cessation. Only four of them maintained a viral load of < 400 RNA copies/ml for 164–202 weeks after stopping therapy and the remaining participants experienced a viral rebound. Determining the mechanisms for long-term control and the sources causing viral rebound may provide important clues in the search for a functional cure.

Because of the risks and limited success cases after the discontinuation of cART, treatment interruption is generally not recommended for HIV-infected patients. Therefore, a better understanding of the mechanisms underlying viral rebound and in vivo evaluation of novel approaches to achieving a functional cure, require the use of animal models for HIV infection (Garcia, 2016; Skelton et al., 2018; Denton et al., 2012; Honeycutt et al., 2017; Kessing et al., 2017; Marsden et al., 2020; Lim et al., 2018). With their affordability, accessibility, and flexibility, humanized mice are appreciated as a powerful tool for this type of research (Garcia, 2016; Skelton et al., 2018). Like most HIV-infected patients, therapy interruption results in a rapid viral rebound in humanized BLT mice with fully suppressed plasma viremia (Denton et al., 2012). Using humanized myeloid-only mice (MoM) in which macrophages serve as the target of HIV infection, Honeycutt et al. (2017) found that 33% of the HIV-infected, virally suppressed mice had viral rebound at 7 weeks after cART interruption. This result indicates that the tissue macrophages can also contribute to viral persistence and subsequent rebound. In Kessing et al. (2017), Kessing et al. demonstrated that combining the Tat inhibitor didehydro-Cortistatin A with ART accelerates HIV suppression and significantly delays viral rebound after treatment interruption in HIV+ humanized BLT mice. Recently, Marsden et al. (2020) proposed another functional cure approach and showed that the administration of latency-reversing agents (LRAs) during ART prevents viral rebound after treatment cessation in humanized BLT mice.

In addition to experimental research, mathematical models have also provided valuable insights into the HIV infection process after treatment interruption (Li and Wang, 2014; Conway and Perelson, 2015; Wang et al., 2017b; Yan and Wang, 2019; Prague et al., 2019; Bing et al., 2020). In Conway and Perelson (2015), Conway and Perelson showed that patients could have the viral rebound, depending on the CTL response strength, the latent reservoir size at treatment termination, and the initial population of infected cells. Wang et al. analytically showed the dynamic behavior of bistability (Wang et al., 2017b), suggesting that patients can either undergo viral rebound after treatment termination or achieve post-treatment control. Li and Wang (2014) investigated an HIV infection model with logistic proliferation for both uninfected and infected cells and showed that the viral rebound can occur in certain parameter regimes. Another modeling study suggested that the joint therapy of inducer and antibodies can lead to a significant delay of viral rebound by reducing the latent reservoir (Yan and Wang, 2019).

In the experimental work (Honeycutt et al., 2017), Honeycutt et al. used humanized MoM to avoid the confounding complications of having an excess of T cells present during the evaluation of HIV persistence in macrophages. They found HIV can persist in macrophages in vivo despite effective treatment. This is consistent with our recent modeling paper (Guo et al., 2020). Moreover, viral rebound was observed within 2 weeks of therapy discontinuation in all BLT mice (Honeycutt et al., 2017). Some questions arise: what are the roles of CD4+ T cells and macrophages in the viral load decline in BLT mice (and patients) during therapy? Do macrophages contribute to viral persistence in the presence of CD4+ T cells? What are the main factors driving viral rebound after treatment cessation and is it possible to delay viral rebound? In this paper, we address these questions by combining the experimental MoM and BLT data from Honeycutt et al. (2017) with two humanized mouse models to distinguish the contributions of macrophage and CD4+ T cells during treatment and viral rebound after treatment cessation. To obtain parameter values and explain the viral decay dynamics during cART, we fit models with different assumptions on viral decay to the viral load data from treated and untreated MoM and BLT mice (Honeycutt et al., 2017). Using the model with best-fitted parameter values, we study the dynamics of viral load and latent cells before and after therapy is stopped, and evaluate if the viral load at the start of treatment and the latent reservoir size at treatment termination are correlated with the time to viral rebound. These results may provide some implications for treatment strategies that aim to delay or even prevent viral rebound after treatment cessation.

2. Models and data fitting

In this section, we study the dynamics of HIV infection in BLT mice. We used the nonlinear least square method for data fitting and parameter estimation. The experimental data from Honeycutt et al. (2017) are the viral load in ART-treated and untreated MoM and BLT mice. We fit these data using the viral load prediction by the models at time t with or without treatment. More specifically, we used a two-step procedure for data fitting and parameter estimation: (1) fit the macrophage infection model (i.e. MoM model) to the viral load data from treated and untreated MoM (Honeycutt et al., 2017); (2) fix the macrophage-related parameter values and fit the model with CD4+ T cell and macrophage infection (i.e. BLT model) to the viral load data from the treated and untreated BLT mice (Honeycutt et al., 2017). The best-fit estimates are the parameter values that minimize the following function

$$\sqrt{\sum_{i=1}^{n}(\log_{10}\tilde{V}_i-\log_{10}\hat{V}_i)^2},$$

where n is the number of data points, $\tilde{V}_i$ is the experimental data of viral load at the ith data point, and $\hat{V}_i$ is the modeling prediction corresponding to the same data point. The estimation of parameters and numerical simulations later are conducted using Matlab R2020b. The codes are available at https://github.com/ronglibin/JTB-MoM-BLT-model.

2.1. MoM model and data fitting

Because CD4+ T cells are not present in MoM (Honeycutt et al., 2016, 2017), we consider the following model with only macrophage infection

$$\begin{cases}\dfrac{dM(t)}{dt}=s_M-d_M M-k_M MV,\\ \dfrac{dM^*(t)}{dt}=k_M MV-\mu_M M^*,\\ \dfrac{dV(t)}{dt}=N_M\mu_M M^*-cV,\end{cases}\tag{1}$$

where $M(t)$, $M^*(t)$ and $V(t)$ are the concentrations of uninfected macrophages, infected macrophages and viruses at time t, respectively. Uninfected macrophages are generated at rate s_M, die at per capita rate d_M, and are infected by the virus at rate k_M. The death rate of infected macrophages is μ_M. The parameter N_M denotes the total number of viruses produced by one infected macrophage in its lifespan. Constant c is the viral clearance rate. The model parameters are assumed to be positive. Model (1) is a basic viral dynamic model as in Perelson et al. (1996) but the target cell is different.

In the Ref. Honeycutt et al. (2017), three antiretroviral drugs, two reverse transcriptase inhibitors (emtricitabine and tenofovir disoproxil

fumarate) and an integrase inhibitor (raltegravir), were administered to eight HIV infected MoM. For all treated MoM, the plasma viral load decreased to below the detection limit of 668 RNA copies/ml within 2 weeks of treatment initiation. In contrast with the high viral load in untreated MoM, triple therapy is effective in inhibiting viral replication in treated MoM. For data fitting, we assume that antiretroviral drugs are 100% effective in blocking virus infection, i.e. $k_M = 0$. Using the method in Perelson et al. (1996, 1997) and Perelson and Nelson (1999), the viral load at time t is given by

$$V(t) = \frac{V_0}{c-\mu_M}[ce^{-\mu_M t} - \mu_M e^{-ct}], \tag{2}$$

where V_0 is the steady-state viral load before therapy. As shown in the supplementary Fig. 3b of Honeycutt et al. (2017), five mice had only one viral load measurement and three mice had two viral load measurements available. Thus, it is challenging to identify all the parameters in formula (2). The experimental paper (Honeycutt et al., 2017) found an average 1.3-log and 1.8-log reduction in plasma viral RNA after 1 week of treatment for BLT and MoM, respectively. This rapid drop in plasma viremia is consistent with the result in humans (Ramratnam et al., 1999). For this reason, we assumed the viral clearance rate to be the same and it is fixed to be $c = 23\ \text{day}^{-1}$. This value was estimated in Ramratnam et al. (1999) and used in other studies (Wang and Rong, 2014; Wang et al., 2017a, 2016; Wang and Rong, 2019; Guo and Qiu, 2019). The remaining two parameters include the baseline viral load V_0 and the death rate of infected macrophages μ_M. Since the data of only three out of eight treated MoM are available in the supplementary Fig. 3b of Honeycutt et al. (2017), we use the average viral load data from the eight MoM (see Fig. 2a of Honeycutt et al. (2017)) in data fitting. On the basis of the best fit, we estimate the death rate of infected macrophages $\mu_M = 0.58\ \text{day}^{-1}$.

By fixing the death rate of infected macrophages from the treated MoM, we fit model (1) to the viral load data of all the six untreated MoM (supplementary Fig. 3a in Honeycutt et al. (2017)) and estimate the remaining parameters, including the generation rate of uninfected macrophages s_M, the death rate of uninfected macrophages d_M, the infection rate of macrophages by free virus k_M, and the viral burst size of an infected macrophage N_M. Because only the viral load is measured in experiment (Honeycutt et al., 2017), the product of two parameters (s_M and N_M) and the remaining two parameters can be estimated. Thus, we make a further assumption on the generation rate of uninfected macrophages s_M. As shown in Fig. 2f of Honeycutt et al. (2017), the mean numbers of human macrophages in the liver, lung, spleen, and bone marrow of MoM are 3.1×10^5, 1.5×10^5, 7.5×10^4 and 1.5×10^6, respectively. Thus, the total number of human macrophages present in examined tissues is 2.035×10^6. Since the adult mouse (ranges from 13 to 48 weeks) has an average volume of 264 ml and the examined tissues account for approximately 10% of the total volume (Shi, 1974), the volume of examined tissues is estimated to be 26.4 ml. Thus, in the absence of infection, the macrophage level is $2.035 \times 10^6/26.4 = 7.71 \times 10^4\ \text{ml}^{-1}$. Assuming the system (1) is at steady state before infection (Wang and Rong, 2014; Wang et al., 2017a), we obtain that the generation rate of uninfected macrophages s_M is $7.71 \times d_M \times 10^4\ \text{ml}^{-1}\ \text{day}^{-1}$. With this parameter value, the best fits are shown in Fig. 1 for six untreated MoM (black solid line). It follows that model (1) provides good fits to the viral load data (Honeycutt et al., 2017). Parameter estimates corresponding to the best fits are given in Table 1.

2.2. BLT model and data fitting

To compare with the experimental results obtained in MoM, Honeycutt et al. (2017) conducted similar experiments in BLT mice. For BLT mice, both CD4+ T cells and macrophages are the target of HIV infection (Honeycutt et al., 2017; Skelton et al., 2018; Wege et al., 2008; Melkus et al., 2006). Thus, we first use a model that includes the infection of both CD4+ T cells and macrophages to fit the viral load data in treated BLT mice. However, the basic model fails to capture the slow viral decline in the later period of suppressive therapy (Fig. 1a of Honeycutt et al. (2017)). The latently infected cells might be a possible reason for such a slow decay (Perelson et al., 1997; Perelson and Ribeiro, 2013). For this reason, we modify the basic model by including latently infected CD4+ T cells and then fit it to the viral load data from BLT mice (Honeycutt et al., 2017). To compare the best fits with different assumptions, the sum of squared residuals (SSR) and the Akaike information criterion (AIC) will be calculated.

2.2.1. Model without latently infected cells

We start with the following model including the infection of both CD4+ T cells and macrophages,

$$\begin{cases} \dfrac{dT(t)}{dt} = s_T - d_T T - (1-\epsilon)k_T TV, \\ \dfrac{dT^*(t)}{dt} = (1-\epsilon)k_T TV - \mu_T T^*, \\ \dfrac{dM(t)}{dt} = s_M - d_M M - (1-g\epsilon)k_M MV, \\ \dfrac{dM^*(t)}{dt} = (1-g\epsilon)k_M MV - \mu_M M^*, \\ \dfrac{dV(t)}{dt} = N_T\mu_T T^* + N_M\mu_M M^* - cV, \end{cases} \tag{3}$$

where $T(t)$ and $T^*(t)$ are the concentrations of uninfected CD4+ T cells and infected CD4+ T cells at time t, respectively. Uninfected CD4+ T cells are generated at rate s_T, die naturally at rate d_T per cell, and become infected by free virus at rate k_T. The constant μ_T is the death rate of infected CD4+ T cells, and N_T is the number of virions produced by one infected CD4+ T cell during its lifetime. Constant ϵ ($0 \le \epsilon \le 1$) is the overall effectiveness of the treatment in blocking virus infection of CD4+ T cells (Rong and Perelson, 2009a). Compared with infected CD4+ T cells, infected macrophages can pump antiretroviral drugs out by using the P-glycoprotein transporter (Kim et al., 1998). Thus, we use $g\epsilon$ to represent the drug efficacy of blocking macrophage infection, where g is the effective penetrance of drugs ranging from 0 (drugs have no effect) to 1 (drugs are as effective as in infected CD4+ T cells). Models with multiple target cell populations have also been used in some other studies (Rong and Perelson, 2009b; Callaway and Perelson, 2002; Perelson et al., 1997). All other variables and parameters are the same as those in model (1).

Similar to the method in Section 2.1, we assume that antiretroviral therapy is 100% effective in blocking the infection of CD4+ T cells and macrophages and that model (3) is at a steady state before treatment. Thus, the viral load after drug therapy can be solved as follows (Perelson et al., 1997):

$$V(t) = \bar{V}[Ae^{-\mu_T t} + Be^{-\mu_M t} + (1-A-B)e^{-ct}], \tag{4}$$

where $A = \frac{N_T k_T \bar{T}}{c-\mu_T}$ and $B = \frac{c-N_T k_T \bar{T}}{c-\mu_M}$. $\bar{T}$ and $\bar{V}$ denote the concentrations of uninfected CD4+ T cells and free virus at steady state before treatment, respectively.

We fit the value of $V(t)$ predicted by Eq. (4) to the viral load data of BLT mice during cART treatment and estimate the parameters (Honeycutt et al., 2017). The viral load data from 4 treated BLT mice were given in supplementary Fig. 1b of Honeycutt et al. (2017). These data only account for a fraction of the 13 treated BLT mice. Thus, we use the average of the data from 13 treated BLT mice (i.e. the data of Fig. 1a in Honeycutt et al. (2017)) to estimate the parameters in (4). The first data point below the detection limit is assumed to be half of the detection limit, i.e. 334 RNA copies/ml. Except for the first data point, other data below the detection limit are not included in our fit. We fix the viral clearance rate c to be $23\ \text{day}^{-1}$. For the death rate of infected CD4+ T cells, we choose the range $0.2 \le \mu_T \le 1.2$, which covers most of the estimates in Refs. Perelson et al. (1996, 1997) and Wu et al. (2008). In general, the source of multiphasic viral load decline during therapy depends on the exponential terms in Eq. (4). Thus, we will discuss the

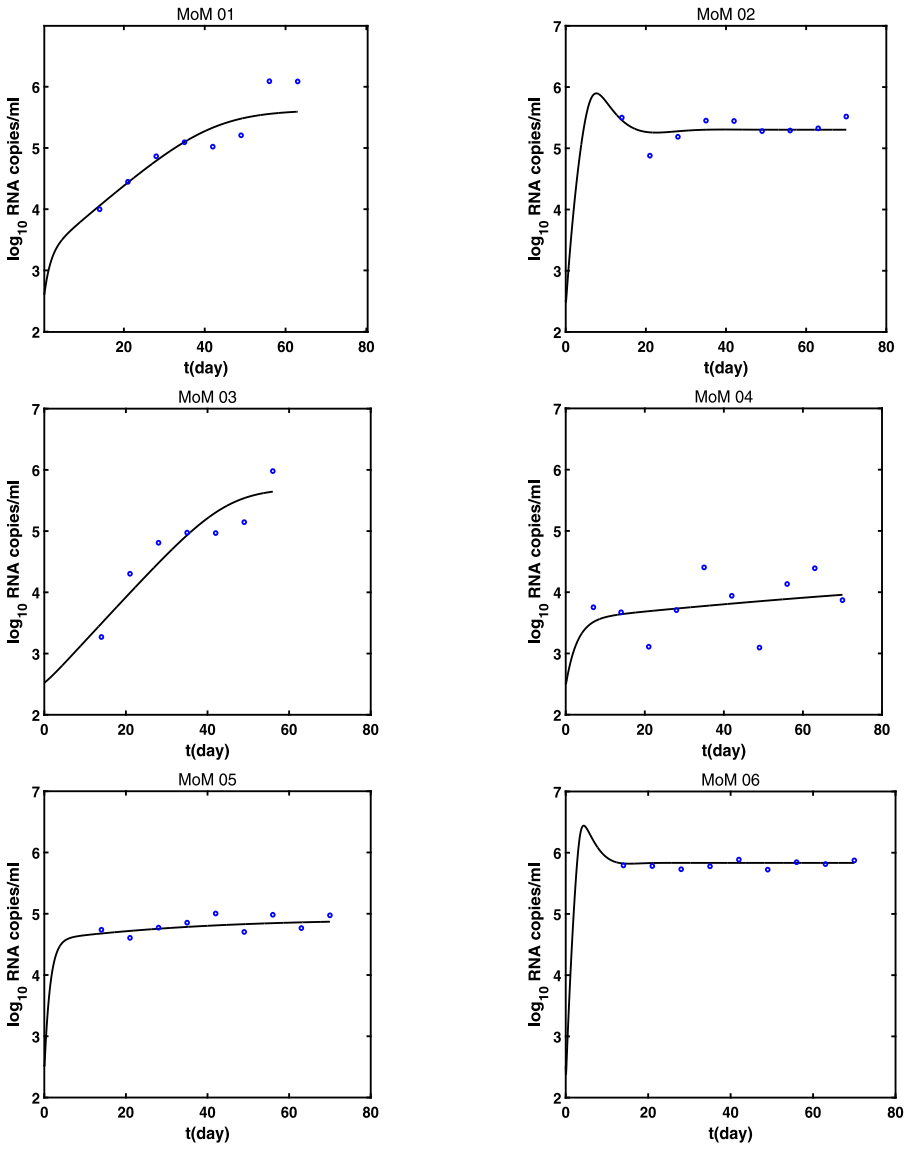

Fig. 1. The best fits of model (1) to the viral load data from six untreated MoM (Honeycutt et al., 2017). The blue circles represent the observed viral load data on the $\log_{10}$-scale, and the black solid lines represent the model predictions. The viral clearance rate is fixed at $c = 23$ day^{-1} and the death rate of infected macrophages is $\mu_M = 0.58$ day^{-1}. The model provides a good fit to the viral load data from six untreated MoM. The parameter values based on the fits are listed in Table 1.

Table 1
Parameter values of the best fits of model (1) to six untreated HIV-infected MoM.

Mice	Death rate of uninfected macrophages d_M (day^{-1})	Infection rate of macrophages by free virus k_M (ml/day)	Viral burst size of infected macrophage N_M (virus/cell)	Generation rate of uninfected macrophages s_M (ml^{-1} day^{-1})
MoM 01	0.649	3.604×10^{-7}	1019	5.004×10^4
MoM 02	0.22	5.336×10^{-7}	837	1.696×10^4
MoM 03	0.489	2.912×10^{-7}	1328	3.77×10^4
MoM 04	0.36	5.093×10^{-7}	604	2.776×10^4
MoM 05	0.749	5.912×10^{-7}	537	5.775×10^4
MoM 06	0.307	5.107×10^{-7}	1246	2.367×10^4
Mean	0.462	4.661×10^{-7}	928.5	3.565×10^4
SD	0.188	1.047×10^{-7}	298.8	1.446×10^4

following two cases on the basis of the range $0.2 \le \mu_T \le 1.2$ and the estimate $\mu_M = 0.58$.

***Case A* : $0.2 \le \mu_T < \mu_M = 0.58$.**

If the death rate of infected macrophages is greater than the death rate of infected CD4+ T cells, we fit Eq. (4) to the viral load data of treated BLT mice (Honeycutt et al., 2017). The best fit is shown in Fig. 2a. Based on the best fit, we estimate the death rate of infected CD4+ T cells $\mu_T = 0.2$ day^{-1} and a composite parameter $N_T k_T \bar{T} = 8.753$. Although our fit can reproduce a significant decrease of the viral load within 4 weeks of treatment, it is unable to capture a subsequent slower phase of viral decay. Thus, the model prediction under the above conditions yields a poor fit to the viral load data.

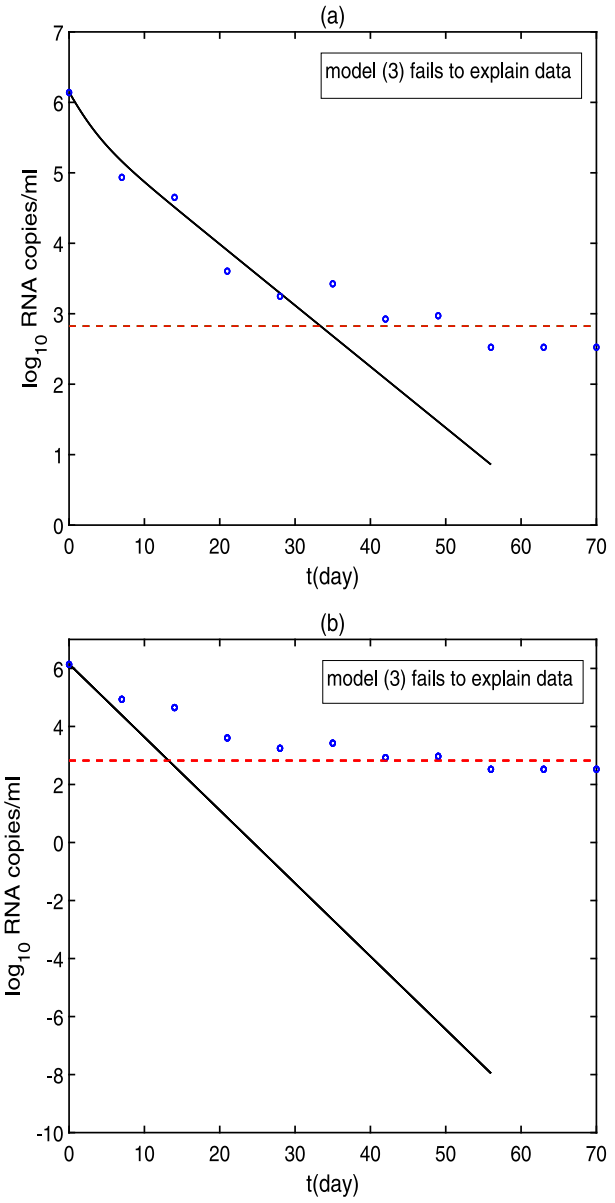

Fig. 2. The mean of the viral load from 13 treated BLT mice (blue circles) compared with the model prediction (black solid line). The fitting assumes that treatment is 100% effective. (a) The death rate of infected CD4+ T cells is assumed to be less than that of infected macrophages, i.e. $0.2 \le \mu_T < \mu_M = 0.58$ day^{-1}. (b) The death rate of infected CD4+ T cells is assumed to be greater than or equal to that of infected macrophages, i.e. $\mu_T \ge \mu_M = 0.58$ day^{-1}. The model fails to reproduce the viral load change (Honeycutt et al., 2017). The viral clearance rate is fixed at $c = 23$ day^{-1}. Data below the detection limit are plotted as half of the detection limit, i.e. 334 RNA copy/ml.

Table 2
Comparison of the best fits under different cases.

Treatment	Figures	SSR	AIC
Yes	Fig. 3a	0.2798	−21.2381
	Fig. 4a	0.9392	−10.3396
No	Fig. 3b	0.8796	−32.7428
	Fig. 4b	1.0066	−30.8547

***Case B* : $0.58 = \mu_M \le \mu_T \le 1.2$.**

When the death rate of infected macrophages is assumed to be less than or equal to that of infected CD4+ T cells, we estimate $\mu_T = 0.58$ day^{-1} and $N_T k_T \bar{T} = 9.435$ by fitting Eq. (4) to the viral load data of treated BLT mice. In this case, we obtain the same death rates for the two types of infected cells. This implies that only one viral decay phase exists in the model prediction, as shown in Fig. 2b (black solid line). However, the viral load in treated BLT mice experiences at least a two-phase decline, as shown in Fig. 1a of Honeycutt et al. (2017). Thus, the model assuming $\mu_M \le \mu_T$ again provides a poor fit to the viral load data (Honeycutt et al., 2017).

In summary, the viral load predicted by Eq. (4) fails to reproduce the experimental data (Honeycutt et al., 2017), no matter if $\mu_T < \mu_M$ or $\mu_T \ge \mu_M$. More specifically, Eq. (4) cannot explain the final slower viral decline in BLT mice during suppressive therapy, as shown in Fig. 2. In Perelson et al. (1997), Perelson and Ribeiro (2013) and Siliciano et al. (2003), the models with the activation of latently infected cells showed a slow viral decay in the later stage of antiretroviral therapy. Thus, we modify the model (3) by including latently infected cells to see if it can improve the fits.

2.2.2. Model with latently infected CD4+ T cells

The model with latently infected CD4+ T cells is given as follows

$$\begin{cases} \dfrac{dT(t)}{dt} = s_T - d_T T - (1-\epsilon)k_T TV, \\ \dfrac{dT^*(t)}{dt} = (1-f)(1-\epsilon)k_T TV + aL - \mu_T T^*, \\ \dfrac{dL(t)}{dt} = f(1-\epsilon)k_T TV - aL - \mu_L L, \\ \dfrac{dM(t)}{dt} = s_M - d_M M - (1-g\epsilon)k_M MV, \\ \dfrac{dM^*(t)}{dt} = (1-g\epsilon)k_M MV - \mu_M M^*, \\ \dfrac{dV(t)}{dt} = N_T \mu_T T^* + N_M \mu_M M^* - cV, \end{cases} \tag{5}$$

where $L(t)$ is the concentration of latently infected CD4+ T cells at time t, f is the fraction of infection that results in latency. Latently infected cells can be activated by relevant antigens to become productively infected cells T^* at rate a, and die at per capita rate μ_L. All the other variables and parameters are the same as those in model (3).

For the convenience of expression, we let $\delta = a + \mu_L$. Using the same assumptions as used for model (3) to derive Eq. (4), we obtain the viral load at time t after treatment initiation

$$V(t) = \bar{V}[Ke^{-\mu_T t} + Le^{-\delta t} + Pe^{-\mu_M t} + (1-K-L-P)e^{-ct}], \tag{6}$$

where

$$\begin{aligned} K &= \frac{N_T k_T \bar{T}}{c-\mu_T}[(1-f) + \frac{af}{\delta} - \frac{af\mu_T}{\delta(\mu_T-\delta)}], \\ L &= \frac{af\mu_T k_T N_T \bar{T}}{\delta(c-\delta)(\mu_T-\delta)}, \\ P &= \frac{1}{c-\mu_M}[c - (1-f)N_T k_T \bar{T} - \frac{af N_T k_T \bar{T}}{\delta}]. \end{aligned} \tag{7}$$

To estimate the parameters in Eq. (6), we fix the viral clearance rate $c = 23$ day^{-1} and the death rate of infected macrophages $\mu_M = 0.58$ day^{-1}. Similar to the Cases A and B in Section 2.2.1, we consider the following two cases.

***Case A* : $0.2 \le \mu_T < \mu_M = 0.58$.**

Similar to Case A in Section 2.2.1, we assume that the death rate of infected CD4+ T cells is less than that of infected macrophages and fit Eq. (6) to the viral load data in treated BLT mice (Honeycutt et al., 2017). The best fit, shown in Fig. 3a, indicates that Eq. (6) agrees with viral load data well. On the basis of the best fit, we estimated $\mu_T = 0.2548$ day^{-1}, $\delta = 0.0548$ day^{-1}, $f = 0.0501$, $af = 0.0006$ and $N_T k_T \bar{T} = 10.9926$. As shown in Fig. 3a, the viral load change is more complex compared with Fig. 2a (i.e. Case A in Section 2.2.1). The viral load decline has three phases. Their slopes of decline are μ_M, μ_T and δ, respectively. This implies that the viral load decline in the first two phases comes from the loss of infected macrophages and productively infected CD4+ T cells. The activation of latently infected CD4+ T cells contributes to the third-phase decline. Moreover, the decay rate of the

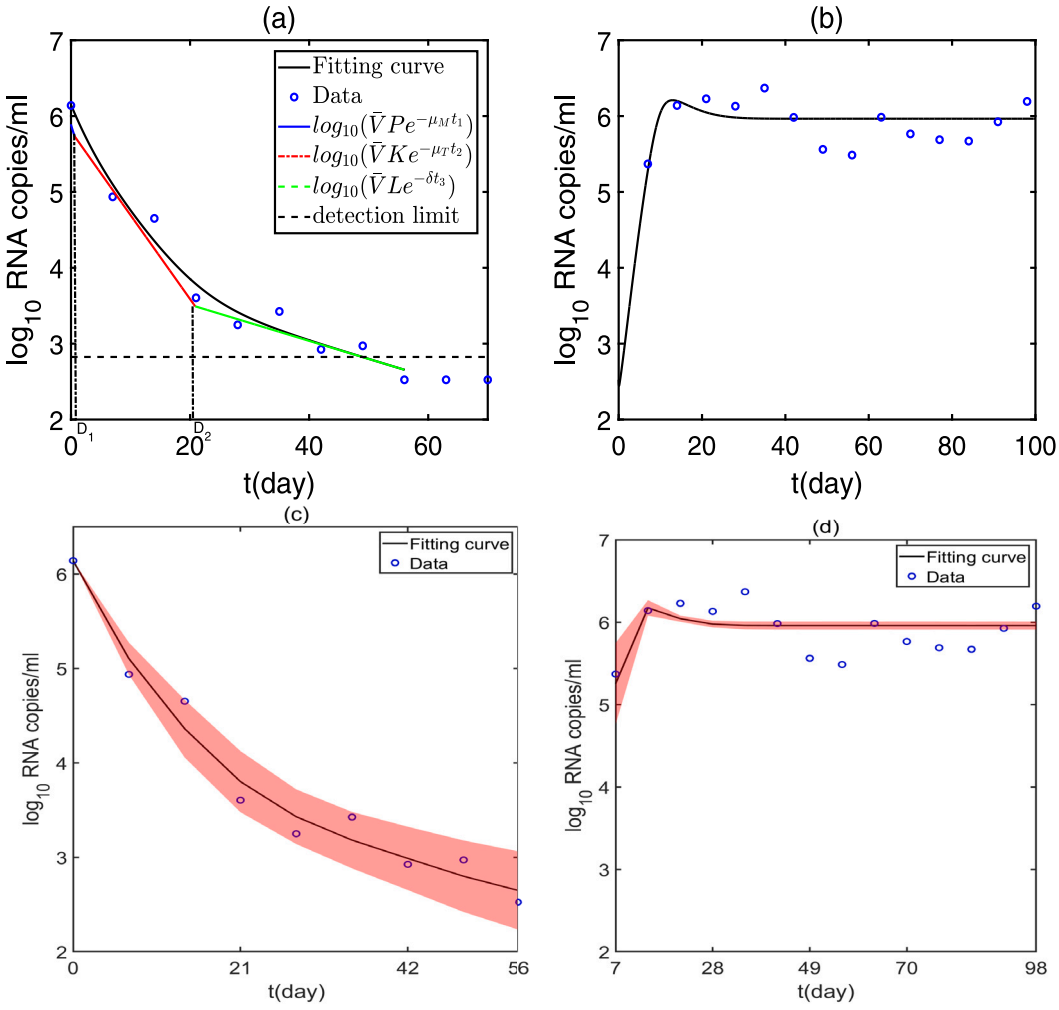

Fig. 3. Model fitting to the viral load data of BLT mice (blue circles). The death rate of infected CD4+ T cells is assumed to be less than that of infected macrophages, i.e. $0.2 \le \mu_T < \mu_M = 0.58$ day^{-1}. (a) Best fit of Eq. (6) (black solid line) to the average data of the 13 treated BLT mice. The viral load decline has three phases, with slopes μ_M, μ_T and δ, respectively. The duration of the first phase D_1 is about 0.59 day and the duration of the second phase D_2 is about 21 days. The horizontal black dashed line represents the detection limit of the polymerase chain reaction assay, i.e. 668 RNA copies/ml. Data below the detection limit are plotted as half of the detection limit. (b) Best fit of model (5) with $\epsilon = 0$ (black solid line) to the average data of the 5 untreated BLT mice. (c,d) The 95% confidence intervals from fitting Eqs. (6) and (5) to the viral data of the treated and untreated BLT mice, respectively. The shaded regions in (c) and (d) denote the 95% confidence interval. The estimated parameters are $\mu_T = 0.2548$ day^{-1} (95% CI: [0.1951, 0.3116]), $\delta = 0.0548$ day^{-1} (95% CI: [0.0409, 0.0678]), $f = 0.0501$ (95% CI: [0.036, 0.0603]), $af = 0.0006$ (95% CI: [0.0005, 0.0007]), $N_T k_T \bar{T} = 10.9926$ (95% CI: [8.5583, 13.3728]), $s_T = 4.65\times10^3$ ml^{-1} day^{-1} (95% CI: [3.704×10^3, 5.655×10^3]), $d_T = 0.1396$ day^{-1} (95% CI: [0.109, 0.172]) and $k_T = 2.1754\times10^{-7}$ day^{-1} (95% CI: [1.647×10^{-7}, 2.711×10^{-7}]).

viral load gradually decreases. By calculating the time at which two curves $log_{10}(Ke^{-\mu_T t})$ and $log_{10}(Pe^{-\mu_M t})$ intersect, we obtain that the first-phase viral decline lasts about half a day (i.e. $D_1 = \frac{\ln(\frac{P}{K})}{\mu_M - \mu_T} = 0.5906$). Similarly, we have the duration of the second phase of viral decline $D_2 = \frac{\ln(\frac{K}{L})}{\mu_T - \delta} = 20.8608$ days. Thus, the first stage of decline lasts much shorter than the later stage during suppressive therapy.

To check the cross-impact of the parameter variations, we randomly draw from the interval of increasing or decreasing the best-fitted parameter values by 20%. According to the Latin Hypercube Sampling (LHS) method, we randomly sample one parameter set of μ_T, δ, f, af and $N_T k_T \bar{T}$ within their ranges and produce 100 different artificial datasets. By analyzing each dataset with Eq. (6), we obtain the 95% confidence interval (CI) for the above five parameters, i.e., μ_T: [0.1951, 0.3116], δ: [0.0409, 0.0678], f: [0.036, 0.0603], af: [0.0005, 0.0007] and $N_T k_T \bar{T}$: [8.5583, 13.3728]. The 100 datasets correspond to 100 curves. Fig. 3c shows 95% CI of the model simulations.

Based on the best fits of MoM model Eq. (1) to the viral load data from six untreated MoM, we have obtained the means of best-fit parameter estimates listed in Table 1, including the generation rate of uninfected macrophages $s_M = 565\times10^4$ ml^{-1} day^{-1}, the death rate of uninfected macrophages $d_M = 0.462$ day^{-1}, the infection rate of macrophages by free virus $k_M = 4.661\times10^{-7}$ ml/day, and the viral burst size of infected macrophage $N_M = 928.5$ virus/cell. From the best fits in Fig. 3a, we have the death rate of infected CD4+ T cells $\mu_T = 0.2548$ day^{-1}, the fraction of infection that results in latency $f = 0.0501$, the activation rate of latently infected cells $a = 0.012$, and the death rate of latently infected cells $\mu_L = \delta - a = 0.0548 - 0.012 = 0.0428$ day^{-1}. To estimate the remaining parameters s_T, d_T, k_T and N_T, we fix the above parameters and fit Eq. (5) with $\epsilon = 0$ to the viral load data of untreated BLT mice. However, as described in Wu et al. (2008), the product of s_T and N_T rather than individual parameters can be identified. Thus, we assume that the viral burst size of infected CD4+ T cells N_T is 2000 virus/cell (Wang et al., 2016). In this case, we obtain the best fit in Fig. 3b, which generates good reproduction of the viral load data from untreated BLT mice (Honeycutt et al., 2017). The 95% CI of the model simulations is shown in Fig. 3d. The three parameters corresponding to the best-fit curve are the generation rate of uninfected CD4+ T cells $s_T = 4.65\times10^3$ ml^{-1} day^{-1} (95% CI: [3.704×10^3, 5.655×10^3]), the death rate of uninfected CD4+ T cells $d_T = 0.1396$ day^{-1} (95% CI: [0.109, 0.172]), and the infection rate of CD4+ T cells by virus

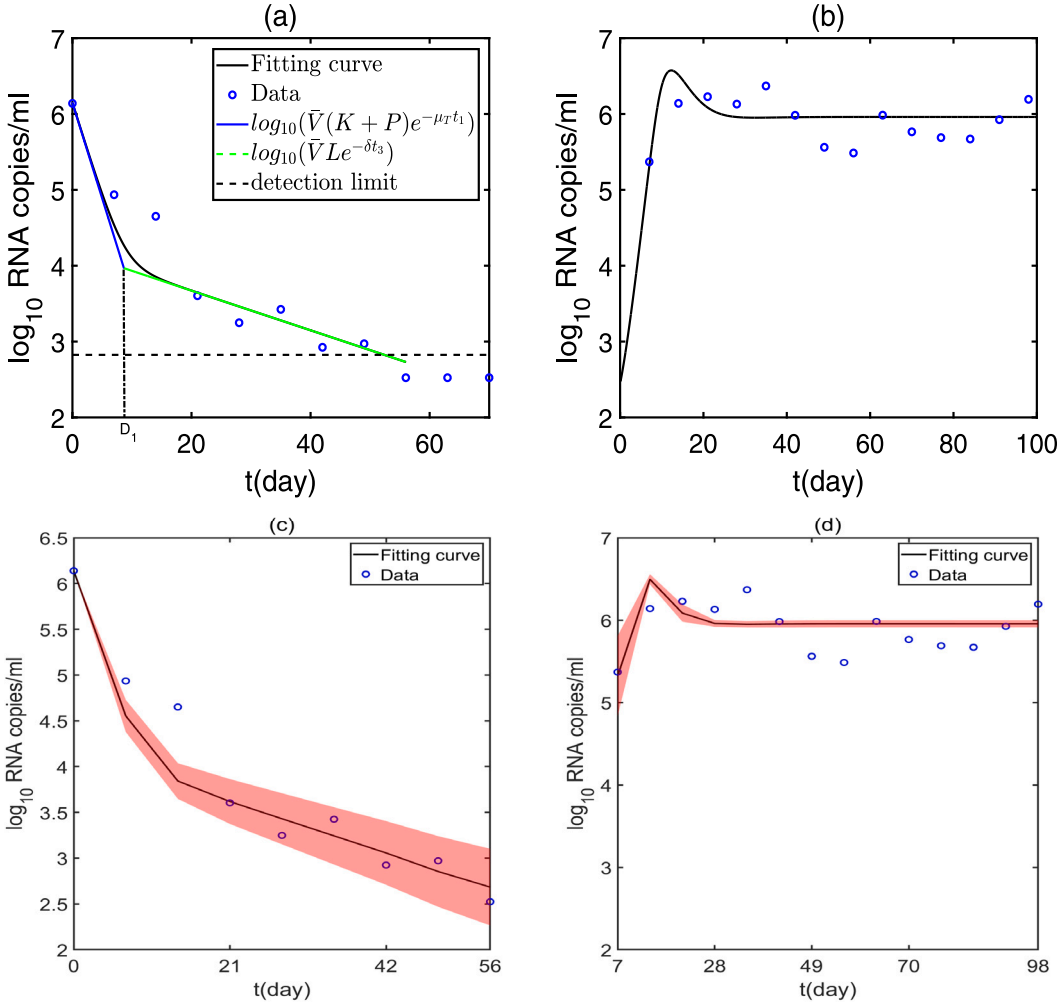

Fig. 4. Model fitting to the viral load data of BLT mice (blue circles). The death rate of infected CD4+ T cells is assumed to be greater than or equal to that of infected macrophages, i.e. $\mu_T \geq \mu_M = 0.58$ day^{-1}. (a) Best fit of Eq. (6) (black solid line) to the average data of the 13 treated BLT mice. The viral load decay has two phases, with slopes μ_T (which was estimated to be equal to μ_M) and δ, respectively. The duration of the first phase D_1 is about 8.6 days. The horizontal black dashed line represents the detection limit. (b) Best fit of model (5) with $\epsilon = 0$ (black solid line) to the average data of the 5 untreated BLT mice. (c,d) The 95% confidence intervals from fitting Eqs. (6) and (5) to the viral data of the treated and untreated BLT mice, respectively. The shaded regions in (c) and (d) denote the 95% confidence interval. The estimated parameters are $\mu_T = 0.58$ day^{-1} (95% CI: [0.4336, 0.7116]), $\delta = 0.0602$ day^{-1} (95% CI: [0.0489, 0.0739]), $f = 0.0461$ (95% CI: [0.0359, 0.0559]), $af = 0.001$ (95% CI: [0.0008, 0.0012]), $N_T k_T \bar{T} = 14$ (95% CI: [10.6939, 17.0892]), $s_T = 3.22 \times 10^3$ ml^{-1} day^{-1} (95% CI: [2.456×10^3, 3.863×10^3]), $d_T = 0.016$ day^{-1} (95% CI: [0.013, 0.02]) and $k_T = 8.051 \times 10^{-8}$ day^{-1} (95% CI: [6.454×10^{-8}, 9.77×10^{-8}]).

$k_T = 2.1754 \times 10^{-7}$ ml/day (95% CI: [1.647×10^{-7}, 2.711×10^{-7}]). Taken together, the results obtained in Fig. 3 indicate that model (5) provides a good fit to the viral load data from treated and untreated BLT mice.

***Case B* : $0.58 = \mu_M \leq \mu_T \leq 1.2$.**

Similar to Case B in Section 2.2.1, we assume that the death rate of infected CD4+ T cells is greater than or equal to that of infected macrophages and fit Eq. (6) to the viral load data in treated BLT mice. The best-fit curve is given in Fig. 4a (black solid lines). In this case, we estimated $\mu_T = 0.58$ day^{-1} (95% CI: [0.4336, 0.7116]), $\delta = 0.0602$ day^{-1} (95% CI: [0.0489, 0.0739]), $f = 0.0461$ (95% CI: [0.0359, 0.0559]), $af = 0.001$ (95% CI:[0.0008, 0.0012]) and $N_T k_T \bar{T} = 14$ (95% CI: [10.6939, 17.0892]). Consistent with the results obtained in Case B of Section 2.2.1, the estimated death rate of infected CD4+ T cells μ_T is equal to the death rate of infected macrophages μ_M. Thus, the viral load declines in a biphasic manner (see Fig. 4a). After an initial viral decline of approximately 8.648 days (i.e. $D_1 = \frac{\ln(\frac{K+P}{L})}{\mu_T - \delta}$) with the slope μ_T, there is a slower second phase decline with the slope δ.

All parameters in model (5), except for the four T cell-related parameters s_T, d_T, k_T and N_T, have been determined. As stated in the previous case, we again fix $N_T = 2000$ virus/cell because it cannot be determined from the parameter s_T. By fitting Eq. (5) with $\epsilon = 0$ to the viral load data in untreated BLT mice, we obtain the values of the remaining three parameters, $s_T = 3.22 \times 10^3$ ml^{-1} day^{-1} (95% CI: [2.456×10^3, 3.863×10^3]), $d_T = 0.016$ day^{-1} (95% CI: [0.013, 0.02]) and $k_T = 8.051 \times 10^{-8}$ day^{-1} (95% CI: [6.454×10^{-8}, 9.77×10^{-8}]). The best-fit curve is plotted in Fig. 4b, which also agrees well with the viral load data. In conclusion, including the latently infected cells in model (3) can improve the fits of the model to the viral load data in BLT mice (Honeycutt et al., 2017).

Based on the different assumptions, Cases A and B in this section provide good fits to the viral load data in treated BLT mice (see Figs. 3a and 4a). Moreover, as shown in Figs. 3b and 4b, two cases also capture the viral load data in untreated BLT mice (Honeycutt et al., 2017). To determine which one of the two cases generates a better model fit, we calculate the values of SSR and AIC. These two values quantify the goodness-of-fit of different model predictions. A lower SSR indicates better fitting and a lower AIC value indicates a better model. The SSR

and AIC are calculated as follows:

$$\text{SSR} = \sum_{i=1}^{n} (\tilde{V}_i - V_i)^2, \qquad \text{AIC} = n \ln(\text{SSR}/n) + 2p, \quad i = 1, 2, \cdots n, \quad (8)$$

where $\tilde{V}_i$ is the experimental measurements of viral load at the ith data point, V_i is the corresponding values predicted by Eq. (6), n is the number of data points and p is the number of parameters. In the fitting to the viral load of treated BLT mice (i.e. Figs. 3a and 4a), $n = 9$ and $p = 5$. For the fits in Figs. 3b and 4b, $n = 14$ and $p = 3$. The values of SSR and AIC based on the best fits are given in Table 2. We find that Fig. 3a has smaller values of SSR and AIC than Fig. 4a, suggesting that the former gives a better fit to the viral load data from treated BLT mice. In the fitting to the viral load data from untreated BLT mice, Fig. 3b has slightly smaller values of SSR and AIC than Fig. 4b but the improvement is not significant. Therefore, model (5) with the condition $\mu_T < \mu_M$ (i.e. Case A) provides a better fit than the model with the condition $\mu_T \geq \mu_M$ (i.e. Case B).

3. Numerical simulations

An interesting result in the experiments of Honeycutt et al. (2017) is that the MoM with viral rebound has a higher pre-ART viral load and a larger total pre-ART viral burden (i.e. the area under the curve for pre-ART viremia), compared with no-rebound MoM. However, in MoM, macrophages are the only target of HIV infection. Thus, a natural question is to study whether viral rebound occurs in BLT mice, which are reconstituted systemically with virtually all human hematopoietic cell types (Garcia, 2016; Maidji et al., 2019). When viral rebound occurs, we can test whether there is a relationship between the time to rebound and the pre-ART viral load as well as the total pre-ART viral burden, and also determine whether the viral rebound time can be affected by other factors, especially latent cells and viral growth rate. Based on these potential factors, we further study how therapeutic strategies may influence the viral rebound time following treatment discontinuation. The values of parameters are the same as those in Case A of Section 2.2.2, i.e. the best-fit parameter estimates.

3.1. Potential factors for viral rebound

As in the experiments in Honeycutt et al. (2017), we let ART be administered on day 35 and then stopped from day 105. There is no drug treatment in the first 35 days. The viral burst size of infected CD4+ T cells N_T is fixed in model fitting to determine the value of s_T. However, the burst size N_T varies from a few hundred virions to tens of thousands for HIV and SIV in patients and rhesus macaques (Haase et al., 1996; Chen et al., 2007). Using a quantitative technique, image analysis, and in situ hybridization, Haase et al. (1996) assessed viral RNA in cellular compartments in lymphoid tissues in blinded cross-sectional and longitudinal studies of nine HIV-1-infected individuals. They approximated N_T to be one-half of the maximum of the range of the number of copies of HIV RNA per mononuclear cell. They also mentioned that N_T might be underestimated because only about 75% of productively infected mononuclear cells were analyzed. The significantly larger values of N_T (i.e., $N_T > 2000$ virus/cell) have been estimated for SIV (Chen et al., 2007), although it is not clear whether the higher burst sizes are suitable for HIV. It is also very likely that the viral burst size varies in BLT mice. To compare the dynamics of viral load and latent cells, we release the assumption on the viral burst size N_T and let it vary, i.e. $N_T = 500, 2000, 5000$ virus/cell in Fig. 5. From Fig. 5a, we see that the viral load rapidly drops to the detection limit during ART, suggesting that ART effectively suppresses HIV infection in all three cases. However, after treatment interruption, viral load quickly rebounds to the pre-therapy level. This shows that with the given parameter values, the BLT mice are predicted to experience a viral rebound, in agreement with the experimental result obtained from BLT mice (Honeycutt et al., 2017). It is noteworthy that the resurgence

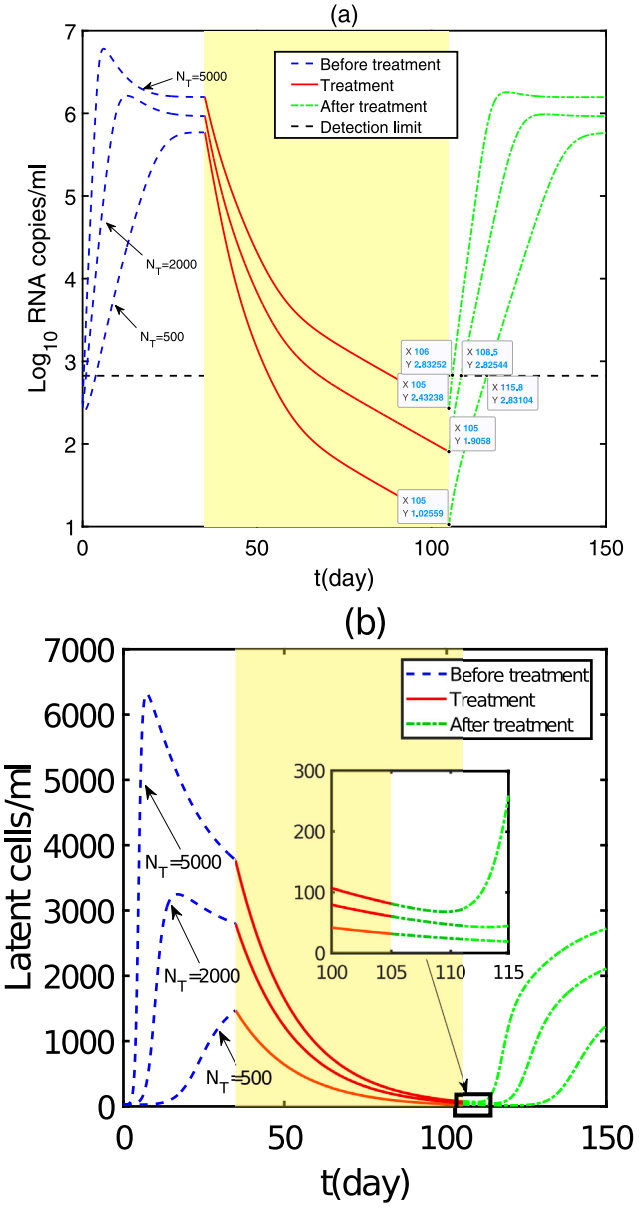

Fig. 5. The dynamics of viral load (a) and latently infected cells (b), predicted by the model (5) with the best-fit parameters. Simulations are performed before antiretroviral therapy (0 to day 35), under antiretroviral therapy (day 35 to 105), and after antiretroviral therapy (after day 105). The time of exposure to ART is indicated with a shaded yellow box. The horizontal black dashed line in (a) represents the detection limit.

of the virus subsequent to treatment discontinuation is an inherently stochastic process. In this study, we employed ordinary differential equations to model this process, which ought to be construed as an approximation of the average outcome.

Biologically, the viral burst size represents the total number of virions produced from one infected cell. Consequently, the viral rebound starts from a lower level for a smaller value of N_T. Following the Ref. Honeycutt et al. (2017), we set the critical level of viral rebound to 668 RNA copies/ml. As shown in Fig. 5a, when $N_T = 500, 2000, 5000$ virus/cell, viral load increases from $10^{1.026}$ RNA copies/ml, $10^{1.906}$ RNA copies/ml and $10^{2.432}$ RNA copies/ml at day 105 to $10^{2.831}$ RNA copies/ml at day 115.8, $10^{2.825}$ RNA copies/ml at day 108.5 and $10^{2.833}$ RNA copies/ml at day 106, respectively. Thus, the viral rebound time is 10.8 days, 3.5 days, and 1 day respectively for $N_T = 500, 2000, 5000$.

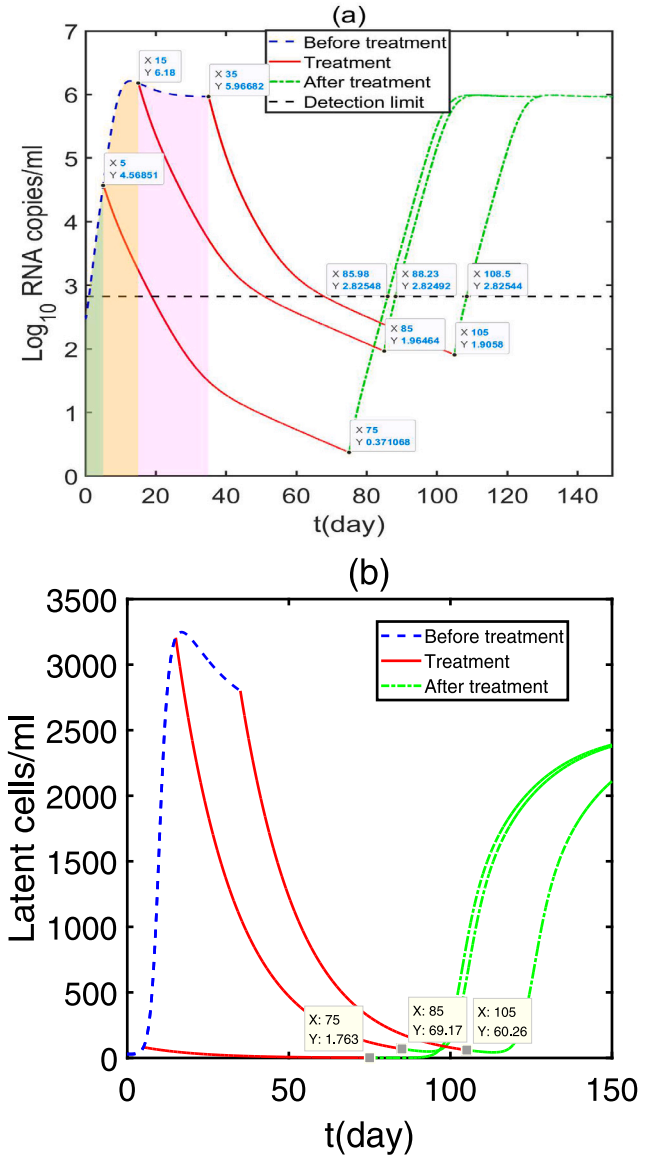

Fig. 6. Viral rebound times with different viral loads at the start of treatment. The dynamics of viral load (a) and latently infected cells (b) are plotted before, during, and after antiretroviral treatment. The pre-ART total viral burdens at different initiate times of ART are represented by the shaded boxes of different colors. The green box, the green and yellow boxes, as well as the boxes with three colors respectively indicate that ART starts on day 5, 15, and 35. The parameters are the same as those in Fig. 3.

From these, we also estimate that the rates of virus growth are about 0.385 day^{-1}, 0.605 day^{-1}, and 0.923 day^{-1} corresponding to the different burst sizes. This means that the time to viral rebound is inversely correlated with the rates of virus growth. In other words, a smaller value of N_T has a smaller viral growth rate after treatment interruption, and thus it takes a longer time for the viral load to rebound to the detection limit. We find that a higher viral load and a total viral burden at the start of treatment are associated with a larger value of N_T (see Fig. 5a). Thus, a higher pre-ART viral load and a larger total pre-ART viral burden lead to a faster viral rebound after ART interruption.

Fig. 5b shows the change of the latent reservoir when $N_T = 500, 2000$ and 5000 virus/cell. Similar to the change of the viral load, latent cells significantly decrease during ART and then increase after therapy interruption. As shown in Fig. 3a, the viral load decline has three phases and the third phase comes from the activation of latently infected cells. As a result, we speculate that the viral rebound after ART cessation may come from the latent reservoir. More specifically, the viral rebound time may be related to the latent reservoir size at treatment termination. To test this hypothesis, we zoom in on the change of latent cells from day 100 to day 115. From the zoom-in figure of Fig. 5b, we can observe that the level of latent cells at treatment termination is higher for a larger N_T. This, together with the results in Fig. 5a, shows that BLT mouse with a lower latent cell count at treatment interruption has a delayed viral rebound. This agrees with the modeling result in Conway and Perelson (2015). It also supports early treatment, which may reduce the latent reservoir size although it is hard to prevent the establishment of the latency. The result is consistent with the observation from the "Mississippi baby" who received potent ART at the age of 30 h and showed a delayed viral rebound after cessation of therapy (Marsden et al., 2020). In summary, the time to viral rebound is postponed when the pre-ART viral load, total pre-ART viral burden, and the size of the latent reservoir at treatment cessation are reduced.

3.2. Therapeutic strategies

To approach a functional cure for HIV infection, one strategy is to significantly prolong the time to viral rebound after treatment cessation. The longer patients have been off treatment without a rebound, the more likely the virus is under control. As discussed in the above section, the reduction in the pre-ART viral load, total pre-ART viral burden, and the size of the latent reservoir at treatment cessation can reduce the viral growth rate, resulting in a delay of the viral rebound. Thus, the strategy may be reducing the value of these three parameters. We consider the following two scenarios.

Scenario A: The initiate time of ART is different, but the duration is the same.

To decrease the pre-ART viral load, total pre-ART viral burden, and the size of the latent reservoir at treatment cessation, we perform numerical simulations with early treatment. For comparison, Fig. 6a presents the dynamics of viral load with different initiate times of ART. Antiretroviral treatment still lasts for 70 days as described above. The rebound time is extended to 10.98 days when the therapy starts on day 5, i.e., viral rebound takes place after day 85.98, which is shown in Fig. 6a. Moreover, the viral load goes from $10^{0.3711}$ RNA copies/ml at day 75 to $10^{2.8255}$ RNA copies/ml at day 85.98, suggesting that the viral growth rate is around 0.515 day^{-1}. When treatment starts on day 15, no viral load is detected within 3.23 days after treatment discontinuation. The values $10^{1.9646}$ RNA copies/ml and $10^{2.8249}$ RNA copies/ml are the viral load at treatment interruption (i.e., day 85) and at the time viral load reached the detection limit (i.e., day 88.23), respectively. This shows that the viral growth rate is about 0.613 per day. If ART starts at day 35, then mice experience a rebound after 3.5 days of treatment cessation. In this case, we estimated the viral growth rate is 0.605 day^{-1} during rebound. According to these results, we see that the earlier the treatment is given, the slower the viral rebound is observed, and thus the longer it takes for the viral rebound to appear. However, viral load rebounds slightly faster when treatment starts on day 15 (i.e., 0.613 day^{-1}), compared with starting treatment on day 35 (i.e., 0.605 day^{-1}). From Fig. 6a, although starting treatment on day 15 has less pre-ART total viral burden than starting treatment on day 35, the pre-ART viral load of the former is higher. Thus, reducing the pre-ART viral load may have a stronger effect than reducing the total pre-ART viral burden in decreasing the viral growth rate and increasing the viral rebound time. In other words, when the pre-ART viral load is high, early treatment is still difficult to delay viral rebound when treatment stops.

Using the same method as in Fig. 6a, we compared the dynamics of latent cells in Fig. 6b. Like the pre-ART viral load, the latent cell level at treatment cessation strongly predicts the rebound time. Indeed, initiating treatment on day 5 has the lowest latent reservoir size at treatment cessation, followed by day 35, and then day 15 (see Fig. 6b). In summary, these results support the early initiation of ART among

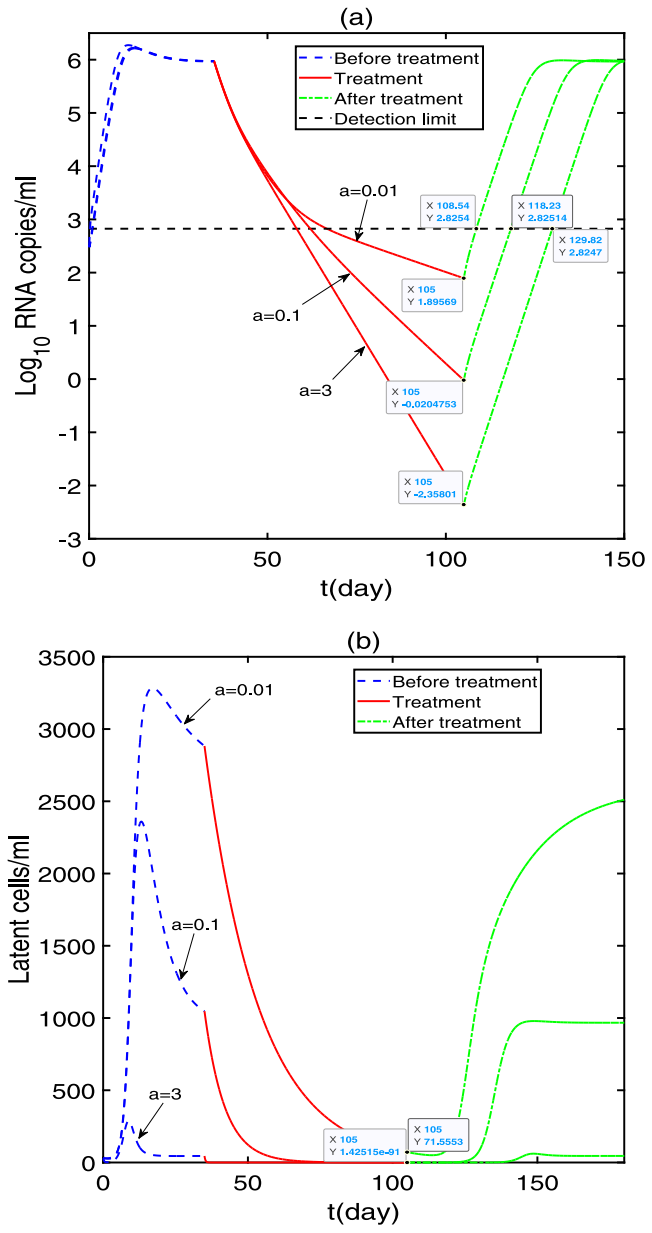

Fig. 7. Sensitivity test of the model (5) with respect to the activation rate of latently infected cells a. The dynamics of viral load (a) and latently infected cells (b) are plotted before, during, and after antiretroviral treatment. The parameter a is assumed to be $a = 0.01, 0.1, 3$ day^{-1}. The other parameters are the same as those in Fig. 3.

HIV-infected patients. In addition, patients with a lower pre-ART viral load have a smaller latent reservoir size at treatment cessation, which increases the viral growth rate and postpones the time to viral rebound after treatment cessation.

From Section 2.2.2, we know that the third-phase viral load (i.e., the low viral load) after suppressive antiretroviral therapy comes from the latent infection of CD4+ T cells. This suggests that the viral rebound after therapy interruption results from latent cells. In model (5), latently infected cells are closely related to the activation rate a in the setting of effective combination therapy. Moreover, it is likely that latently infected cells have different responses to heterogeneous antigens (Rong and Perelson, 2009c). Thus, to test the sensitivity of viral load and the latent reservoir size with respect to a, we plot the viral load and cell changes with different activation constants a in Fig. 7a and b. Based on the previous modeling literature (Rong and Perelson, 2009c,b; Wang and Rong, 2014), the activation rate of latent cells is chosen to be $a = 0.01, 0.1, 3$ day^{-1}. We fix the starting time of antiviral treatment to day 35, in agreement with the study design in experiment (Honeycutt et al., 2017). With a increasing from $a = 0.01$ day^{-1} to $a = 3$ day^{-1}, more latently infected cells are activated, resulting in a slightly higher viral load before cART initiation (see Fig. 7a). When $a = 0.01$ day^{-1}, viral load varies from $10^{1.8957}$ to $10^{2.8254}$ RNA copies/ml at 3.54 days after treatment interruption. The growth rate of the virus is approximately 0.605 day^{-1}. With a larger a, viral rebound occurs after a longer period following cART interruption, corresponding to a smaller viral growth rate (i.e., 0.495 and 0.481 day^{-1} for $a = 0.1$ and $a = 3$ day^{-1}, respectively). In Fig. 7b, when $a = 0.01$ day^{-1}, the population of latently infected cells is about 71 cells/ml at the time of cART cessation. As the activation rate a increases, the number of latently infected cells decreases. In summary, there is an inverse relationship between the activation rate a of latently infected cells and the viral growth rate or the latent reservoir size at treatment termination.

Scenario B: The initiate time of ART is the same, but the duration is different.

For a given initial value of the viral load, we study the effect of longer treatment on the latent cell level at treatment cessation and the time to viral rebound. ART is assumed to be maintained for 70, 100, and 150 days, respectively in Fig. 8a. When the treatment lasts for 150 days, the viral rebound time is 12.82 days. During this period, viral load increases from $10^{0.0017}$ RNA copies/ml to $10^{2.8267}$ RNA copies/ml, and thus the viral growth rate is about 0.507 day^{-1}. The rebound times corresponding to 70 and 100 days of treatment are 3.5 and 6.917 days, respectively. Similarly, we can show that the growth rates of virus are 0.544 and 0.605 day^{-1} respectively for the 70 and 100 days of treatment. In Fig. 8b, the latent reservoir size at treatment cessation is higher for a shorter treatment period. These results show that there is an inverse correlation between the duration of treatment and the growth rate of the virus/the size of the latently-infected population at the end of antiretroviral therapy. Thus, a prolonged treatment period plays an important role in reducing the latent reservoir, slowing down the viral growth and prolonging the rebound time. In conclusion, early ART initiation and longer ART duration can delay the time to viral rebound after treatment cessation.

4. Conclusion and discussion

Different types of humanized mice models have been used and they provided excellent platforms for the analysis of HIV latency, persistence, reactivation, and eradication (Horwitz et al., 2013; Denton et al., 2014; Honeycutt et al., 2013; Seay et al., 2015). BLT mice are reconstituted with human T cells and macrophages, both of which are targets of HIV infection in vivo. By fitting the basic model, i.e. model (3), with the infection of two target cell populations to the viral load data from BLT mice, we find that model (3) is unable to capture the viral decay dynamics observed in treated BLT mice, regardless of the relative magnitude of the death rates of infected CD4+ T cells and macrophages (Fig. 2). To address this issue, we include the latently infected CD4+ T cells in model (3). As expected, the model (3) with latently infected CD4+ T cells (i.e. model (5)) agrees with the viral load data in treated and untreated BLT mice well (Figs. 3 and 4). Moreover, it follows from Table 2 that Fig. 3 provides a better fit than Fig. 4 in fitting the viral load data in treated and untreated BLT mice. The viral load decline has three distinct phases (Fig. 3). In the third phase, viral load is suppressed to below the detection limit. According to the fitting result in Fig. 3, the virions in the third phase result from the activation of latently infected CD4+ T cells. This suggests that latently infected CD4+ T cells may be the reason for the viral rebound observed in BLT mice after therapy interruption (Honeycutt et al., 2017). It is worth noting that when estimating the parameters using the MoM model (1), we fit the model to the individual viral load data of all the six untreated MoM (Fig. 1). Model (1) provides good fits to the viral load data, although the fitted curves have different trends. The parameter

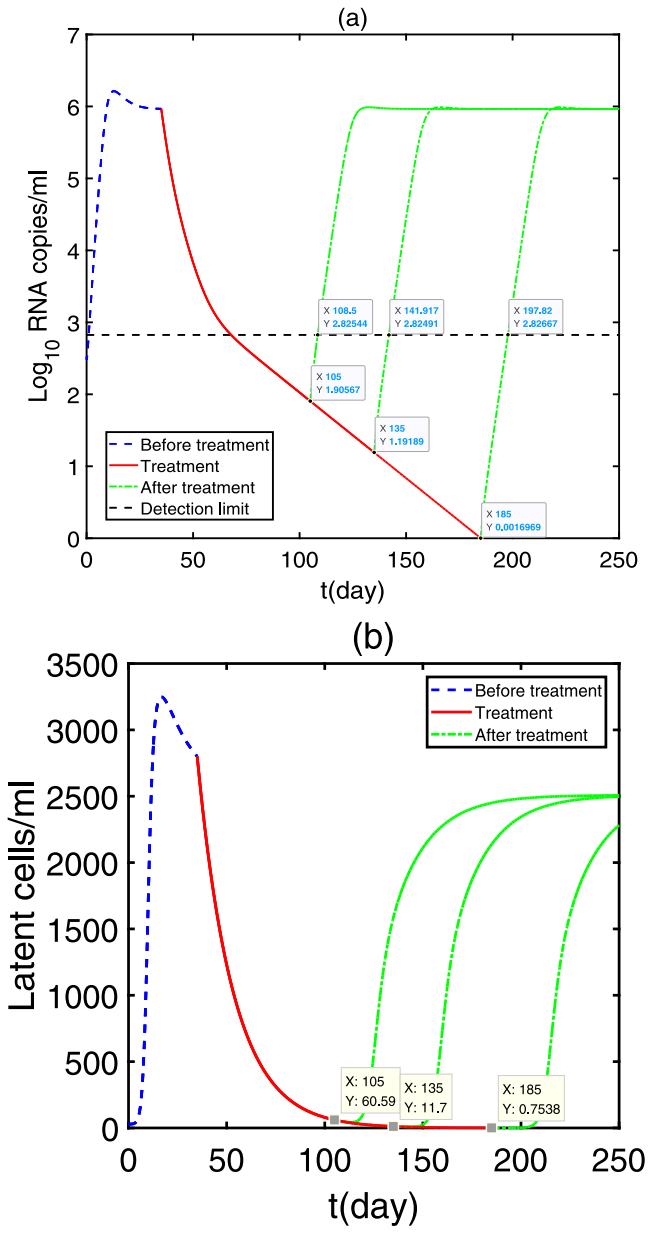

Fig. 8. The effect of varying the treatment duration on the time to viral rebound. The dynamics of viral load (a) and latently infected cells (b) are plotted before, during, and after antiretroviral treatment. The parameters are the same as those in Fig. 3.

estimates are given in Table 1. For each parameter, although different mice have different estimates, the deviation between them is not large. For the BLT mice, we had to use the average data for fitting due to limited data available for each mouse. Thus, the fitting cannot capture the inter-individual variation of mice. According to the fitting results to individual data in MoM, we speculate that the fitting to the individual data of BLT would be similar to the average data and the following conclusion remains unchanged: (1) including the latently infected cells in model (3) can improve the fits of the model to the viral load data in BLT mice; (2) viral persistence under treatment may be due to the latent infection of CD4+ T cells.

Latently infected CD4+ T cells can escape antiretroviral treatment and immune surveillance and are considered a major obstacle to viral elimination. In this paper, the half-life of the latently infected CD4+ T cells (i.e. $\ln 2/\mu_L$) is about 16.2 days. These cells may decay at a slower rate and thus have a longer half-life in patients under long-term suppressive therapy (Siliciano et al., 2003; Ramratnam et al., 2000). In an experimental study, Chomont et al. (2009) showed that the stability of latent reservoir can be maintained by the homeostatic proliferation of latently infected cells. A logistic term representing the homeostatic proliferation has also been employed in some mathematical models (Rong and Perelson, 2009b; Wang et al., 2017a; Wang and Rong, 2019; Guo et al., 2021). In this paper, we did not include the logistic term of latently infected cells due to limited viral load data for model validation.

The time to viral rebound is associated with the latent reservoir size at treatment cessation. A small latent reservoir size would increase the predicted time to rebound (Fig. 5). Thus, reducing the latent reservoir has the priority in controlling the virus. A strategy to activate the latency involves the use of latency reversal agents (LRAs), such as auranofin (Shytaj et al., 2012), histone deacetylase inhibitors (Shirakawa et al., 2013), DNA methylase inhibitors (Kauder et al., 2009), and activators of protein kinase C (Archin and Margolis, 2014). However, some studies have shown that LRAs (i.e. "shock" strategy) alone can activate latent cells, but may not be sufficient to purge the latent reservoir (Vaidya and Rong, 2017; Halper-Stromberg and Nussenzweig, 2016). The "shock and kill" strategy needs more investigation.

Viral rebound occurs in BLT mice after the interruption of treatment, as shown in Fig. 5a. From Figs. 6 and 8, we find that an earlier and longer treatment plays an important role in reducing the latent cell level at treatment cessation. Consequently, when treatment stops, the time to viral rebound time is largely postponed. In addition to delaying the time to viral rebound, early treatment might also help to limit viral diversity, offer protection of innate immunity, and accelerate immune restoration (Delwart et al., 2002; Alter et al., 2005; Hecht et al., 2006). Wolfgang et al. (2013) showed that a longer ART duration in primary HIV infection is also associated with a higher probability of viral control after ART stops. Altogether, these results suggest that early and long-term treatment provides significant benefits to HIV-infected patients.

By fitting model (1) to the viral load data of treated MoM, we estimated that the death rate of infected macrophages μ_M is 0.58 day^{-1}. This means that infected macrophages have a half-life of about 1.19 days. Similar estimates for the half-life of infected macrophages have been obtained by Micci et al. (2014) and Honeycutt et al. (2017). Given the short half-life of infected macrophages during ART treatment, it is possible that no rebound is expected after ART interruption, which was the case for 67% of the ART-treated MoM in the Ref. Honeycutt et al. (2017). However, 33% of the virally suppressed MoM still had viral rebounds after therapy interruption. This implies that some other factors may lead to viral persistence and subsequent viral rebound. The long-lived macrophages, such as microglial cells and astrocytes in the central nervous system, could be an explanation. These cells can live from weeks to decades despite effective treatment and thus contribute to viral persistence and re-establishment of productive infection after treatment interruption (Reu et al., 2017). Using the macaque model of HIV infection, Avalos et al. (2017) showed that latently infected microglial cells persist in most suppressed macaques. They further found that the virions produced by these microglial cells are infectious and replication-competent. Thus, latently infected macrophages may be a source of a viral rebound during treatment interruption. Unfortunately, no information on the latent macrophages was given in the experimental study in mice (Honeycutt et al., 2017). For this reason, we did not include the latent macrophage pool in the model.

To make the fitted parameters (the death rate of infected macrophages μ_M, the death rate of infected CD4+ T cells μ_T, the total loss rate of latently infected CD4+ T cells δ) well separated, we assume that cART is sufficiently effective, as used in many other modeling studies to estimate parameters (Perelson et al., 1997, 1996; Perelson and Nelson, 1999). In this case, we study the dynamics and sources of viral load in the multiple distinct phases, and mathematically obtain the duration each phase lasts. In the numerical simulations (Section 3), the dynamics of the virus and latent cells are described

under three different conditions, namely, no treatment, perfect treatment, and drug withdrawal. We also obtain the relationship between the time to rebound and the pre-ART viral load, latent cells, and viral growth rate. If the treatment is not 100% effective, then viral replication continues throughout cART treatment, bringing a high risk of drug-resistant viral mutants (Mansky and Temin, 1995). However, the studies on the existence of ongoing viral replication during cART presented contradictory evidence. For example, limited viral evolution during ART (Kieffer et al., 2004; Joos et al., 2008) and unsuccessful treatment intensification (Gandhi et al., 2010; Dinoso et al., 2009) both suggest that the level of ongoing viral replication is minimal. Thus, we assumed that antiretroviral therapy is very effective in blocking viral infection. The estimated values of μ_M, μ_T, and δ with this assumption would be the minimal estimates. Although we can distinguish different mechanisms of ART's actions (such as blocking infection or reducing viral production) in the model, it is difficult, if not impossible, to estimate their efficiency based on the available viral load change data.

This paper and Conway and Perelson (2015) both study the time to viral rebound but the models and focus are different. The Ref. Conway and Perelson (2015) focuses on the potential effect of immune response on the post-treatment control of HIV infection in humans using a model with only CD4+ T cell infection. Our model is developed based on the reconstituted features of humanized mice. Macrophages are the only target of HIV infection in humanized MoM while CD4 and macrophages both are the targets of infection in BLT. Our models include them (from simple to complex) and model predictions are fitted to multiple datasets in different mice. Rong and Perelson (2009b,c) used models and simulations to explain the overall long-term dynamics during HIV treatment, such as viral persistence, the latent reservoir stability, and viral blips, without comparing with any specific dataset. Here we distinguish the roles of the two target cell populations in different mice and fit the models to the data. Based on the fitting results, we further study the rebound dynamics after treatment interruption. Taken together, the phenomena of low viral load persistence during suppressive antiretroviral therapy and viral rebound after treatment cessation have also been observed in patients and investigated with models. However, the studies of HIV infection in humans are often complicated by the existence of multiple target cells such as CD4+ T cells and macrophages. In this paper, we distinguish these two target cell populations and fit the models to the viral load data in MoM and BLT mice. Some conclusions agree with previous modeling results for patients but this work might be the first time (to the best of our knowledge) using models to investigate the potential roles of various target cells in HIV infection dynamics in mice.

Although we can include immune responses such as CD8+ T cell response in the model for BLT mice (i.e. add another equation of CD8 to the model), there are no immune data available from those mice for model validation (Honeycutt et al., 2017). A recent study shows that the addition of model details without data support might lead to substantial uncertainties because it generally increases the number of influential parameters and the order of the highest-order effect active in the model (Puy et al., 2022). For this reason, we did not include immune responses explicitly in the model when studying the viral load dynamics. Alternatively, the immune effect can be considered to be included in the infected cell death rate or viral clearance rate.

Like other animal models for biomedical research, there are limitations for humanized mice in the study of HIV infection. One of them is the relatively low volume of blood plasma, which leads to a reduced ability in measuring virus suppression below a threshold of 668 RNA copies/ml (Honeycutt et al., 2017). Other limitations include the limited number of peripheral blood cells, and the relatively short lifespan of these animals (Garcia, 2016). However, these limitations may not affect the main findings of the present work: (1) the latent infection of CD4+ T cells can be a source contributing to HIV persistence during suppressive therapy; (2) the latent cell count at treatment interruption and pre-ART viral load are reversely correlated with the time to viral rebound after ART interruption; (3) earlier ART initiation and longer treatment duration can delay HIV rebound. Humanized mice provide an accelerated model for the evaluation of relevant interventions in treating HIV infection.

CRediT authorship contribution statement

Ting Guo: Conceptualization, Methodology, Formal analysis, Writing – original draft. **Qi Deng:** Methodology, Writing – original draft. **Zhipeng Qiu:** Methodology, Writing – original draft, Supervision. **Libin Rong:** Conceptualization, Methodology, Writing – review & editing, Supervision.

Declaration of competing interest

The authors declare that they have no known competing financial interests or personal relationships that could have appeared to influence the work reported in this paper.

Acknowledgments

This work was initiated when T. Guo visited the Mathematics Department of the University of Florida. T. Guo was supported by the Changzhou Scientific and Technological Program grant (CJ20220134), the Natural Science Foundation of Jiangsu Higher Education (22KJB110007), and the National Natural Science Foundation of China (12201077). Q. Deng was supported by the CSC (202006840122) and the Postgraduate Research and Practice Innovation Program of Jiangsu Province (KYCX21_0250). Z. Qiu was supported by the National Natural Science Foundation of China (12071217). L. Rong was supported by the National Science Foundation grant DMS-1950254.

References

Aiamkitsumrit, B., Sullivan, N.T., Nonnemacher, M.R., et al., 2015. Human immunodeficiency virus type 1 cellular entry and exit in the T lymphocytic and monocytic compartments: mechanisms and target opportunities during viral disease. Adv. Virus Res. 93, 257–311.

Alter, G., Teigen, N., Davis, B., et al., 2005. Sequential deregulation of NK cell subset distribution and function starting in acute HIV-1 infection. Blood 106, 3366–3369.

Archin, N., Margolis, D., 2014. Emerging strategies to deplete the HIV reservoir. Curr. Opin. Infect. Dis. 27 (1), 29–35.

Avalos, C., Abreu, C., Queen, S., et al., 2017. Brain macrophages in simian immunodeficiency virus-infected, antiretroviralsuppressed macaques: a functional latent reservoir. Mbio. 8, e01186–17.

Barton, K.M., Burch, B.D., Soriano-Sarabia, N., et al., 2013. Prospects for treatment of latent HIV. Clin. Pharmacol. Ther. 93, 46–56.

Bing, A., Hu, Y., Prague, M., et al., 2020. Comparison of empirical and dynamic models for HIV viral load rebound after treatment interruption. Stat. Commun. Infect. Dis. 12 (Suppl 1), 20190021.

Bol, S.M., van Remmerden, Y., Sietzema, J.G., et al., 2009. Donor variation in in vitro HIV-1 susceptibility of monocyte-derived macrophages. Virology 390, 205–211.

Callaway, D.S., Perelson, A.S., 2002. HIV-1 infection and low steady state viral loads. Bull. Math. Biol. 64, 29–64.

Chen, H.Y., Mascio, M.D., Perelson, A.S., et al., 2007. Determination of virus burst size in vivo using a single-cycle SIV in rhesus macaques. Proc. Natl. Acad. Sci. USA 104 (48), 19079–19084.

Chomont, N., El-Far, M., Ancuta, P., et al., 2009. HIV reservoir size and persistence are driven by t cell survival and homeostatic proliferation. Nature Med. 15, 893–900.

Chun, T.W., Justement, J.S., Lempicki, R.A., et al., 2003. Gene expression and viral prodution in latently infected, resting CD4+ T cells in viremic versus aviremic HIV-infected individuals. Proc. Natl. Acad. Sci. USA 100, 1908–1913.

Collier, A.C., Coombs, R.W., Schoenfeld, D.A., et al., 1996. Treatment of human immunodeficiency virus infection with saquinavir, zidovudine, and zalcitabine. N. Engl. J. Med. 334, 1011–1017.

Conway, J., Perelson, A., 2015. Post-treatment control of HIV infection. Proc. Natl. Acad. Sci. USA 112 (17), 5467.

Delwart, E., Magierowska, M., Royz, M., et al., 2002. Homogeneous quasispecies in 16 out of 17 individuals during very early HIV-1 primary infection. AIDS 16, 189–195.

Denton, P., Long, J., Wietgrefe, S., et al., 2014. Targeted cytotoxic therapy kills persisting HIV infected cells during ART. PLoS Pathog. 10 (1), e1003872.

Denton, P., Olesen, R., Choudhary, S., et al., 2012. Generation of HIV latency in humanized BLT mice. J. Virol. 86 (1), 630–634.

Dinoso, J.B., Kim, S.Y., Wiegand, A.M., et al., 2009. Treatment intensification does not reduce residual HIV-1 viremia in patients on highly active antiretroviral therapy. Proc. Natl. Acad. Sci. USA 106 (23), 9403.

Furtado, M.R., Callaway, D.S., Phair, J.P., et al., 1999. Persistence of HIV-1 transcription in peripheral-blood mononuclear cells in patients receiving potent antiretroviral therapy. N. Engl. J. Med. 340, 1614–1622.

Gandhi, R.T., Zheng, L., Bosch, R.J., et al., 2010. The effect of raltegravir intensification on low-level residual viremia in HIV-infected patients on antiretroviral therapy: a randomized controlled trial. PLoS Med. 7 (8), e1000321.

Garcia, J., 2016. In vivo platforms for analysis of HIV persistence and eradication. J. Clin. Invest. 126 (2), 424–431.

Gorry, P.R., Francella, N., Lewin, S.R., et al., 2014. HIV-1 envelope-receptor interactions required for macrophage infection and implications for current HIV-1 cure strategies. J. Leukoc. Biol. 95, 71–81.

Guo, T., Qiu, Z., 2019. The effects of CTL immune response on HIV infection model with potent therapy, latently infected cells and cell-to-cell transmission. Math. Biosci. Eng. 16, 6822–6841.

Guo, T., Qiu, Z., Rong, L., 2020. Modeling the role of macrophages in hiv persistence during antiretroviral therapy. J. Math. Biol. 81, 369–402.

Guo, T., Qiu, Z., Shen, M., et al., 2021. Dynamics of a new HIV model with the activation status of infected cells. J. Math. Biol. 82, 51.

Haase, A.T., Henry, K., Zupancic, M., et al., 1996. Quantitative image analysis of HIV-1 infection in lymphoid tissue. Science 274 (5289), 985–989.

Halper-Stromberg, A., Nussenzweig, M., 2016. Towards HIV-1 remission: potential roles for broadly neutralizing antibodies. J. Clin. Investig. 126, 415–423.

Hecht, F., Wang, L., Collier, A., et al., 2006. A multicenter observational study of the potential benefits of initiating combination antiretroviral therapy during acute HIV infection. J. Infect. Dis. 194, 725–733.

Hocqueloux, L., Prazuck, T., Avettand-Fenoel, V., et al., 2010. Long-term immunovirologic control following antiretroviral therapy interruption in patients treated at the time of primary HIV-1 infection. AIDS 24, 1598–1601.

Honeycutt, J.B., Thayer, W.O., Baker, C., et al., 2017. HIV persistence in tissue macrophages of humanized myeloid-only mice during antiretroviral therapy. Nature Med. 23, 638–643.

Honeycutt, J., Wahl, A., Archin, N., et al., 2013. HIV-1 infection, response to treatment and establishment of viral latency in a novel humanized T cell-only mouse (TOM) model. Retrovirology 10 (1), 121.

Honeycutt, J.B., Wahl, A., Baker, C., et al., 2016. Macrophages sustain HIV replication in vivo independently of T cells. J. Clin. Invest. 126, 1353–1366.

Horwitz, J., Halper-Stromberg, A., Mouquet, H., et al., 2013. HIV-1 suppression and durable control by combining single broadly neutralizing antibodies and antiretroviral drugs inhumanized mice. Proc. Natl. Acad. Sci. USA 110 (41), 16538–16543.

Joos, B., Fischer, M., Kuster, H., et al., 2008. HIV rebounds from latently infected cells, rather than from continuing low-level replication. Proc. Natl. Acad. Sci. USA 105 (43), 16725–16730.

Katlama, C., Deeks, S.G., Autran, B., et al., 2013. Barriers to a cure for HIV: new ways to target and eradicate HIV-1 reservoirs. Lancet 381, 2109–2117.

Kauder, S., Bosque, A., Lindqvist, A., et al., 2009. Epigenetic regulation of HIV-1 latency by cytosine methylation. PLoS Pathog. 5 (6), e1000495.

Kessing, C., Nixon, C., Li, C., et al., 2017. In vivo suppression of HIV rebound by Didehydro-Cortistatin A, a block-and-lock strategy for HIV-1 treatment. Cell Rep. 21 (3), 600.

Kieffer, T.L., Finucane, M.M., Nettles, R.E., et al., 2004. Genotypic analysis of HIV-1 drug resistance at the limit of detection: virus production without evolution in treated adults with undetectable HIV loads. J. Infect. Dis. 189 (8), 1452–1465.

Kim, R.B., Fromm, M.F., Wandel, C., et al., 1998. The drug transporter P-glycoprotein limits oral absorption and brain entry of HIV-1 protease inhibitors. J. Clin. Invest. 101, 289–294.

Levy, J.A., 2001. The importance of the innate immune system in controlling HIV infection and disease. Trends Immunol. 22, 312–316.

Li, M., Wang, L., 2014. Backward bifurcation in a mathematical model for HIV infection in vivo with anti-retroviral treatment. Nonlinear Anal.-Real 17, 147–160.

Lim, S.Y., Osuna, C.E., Hraber, P.T., et al., 2018. TLR7 agonists induce transient viremia and reduce the viral reservoir in SIV-infected rhesus macaques on antiretroviral therapy. Sci. Transl. Med. 10 (439), eaao4521.

Maidji, E., Moreno, M., Rivera, J., et al., 2019. Cellular HIV reservoirs and viral rebound from the lymphoid compartments of 4'-Ethynyl-2-Fluoro-2'-Deoxyadenosine (EFdA)-suppressed humanized mice. Viruses 11 (3), 256.

Maldarelli, F., 2011. Targeting viral reservoirs: ability of antiretroviral therapy to stop viral replication. Curr. Opin. HIV AIDS 6, 49–56.

Mansky, L.M., Temin, H.M., 1995. Lower in vivo mutation-rate of human immunodeficiency virus type-1 than that predicted from the fidelity of purified reverse-transcriptase. J. Virol. 69, 5087–5094.

Marsden, M., Zhang, T., Du, Y., et al., 2020. Tracking HIV rebound following latency reversal using barcoded HIV. Cell Rep. Med. 1 (9), 100162.

Melkus, M.W., Estes, J.D., Padgett-Thomas, A., et al., 2006. Humanized mice mount specific adaptive and innate immune responses to EBV and TSST-1. Nature Med. 12, 1316–1322.

Micci, L., Alvarez, X., Iriele, R.I., et al., 2014. CD4 depletion in SIV-infected macaques results in macrophage and microglia infection with rapid turnover of infected cells. PLoS Pathog. 10, e1004467.

Okoye, A.A., Picker, L.J., 2013. CD4+ T cell depletion in HIV infection: mechanisms of immunological failure. Immunol. Rev. 254, 54–64.

Palmer, S., Maldarelli, F., Wiegand, A., et al., 2008. Low level viremia persists for at least 7 years in patients on suppressive antiretroviral therapy. Proc. Natl. Acad. Sci. USA 105, 3879–3884.

Perelson, A.S., Essunger, P., Cao, Y., et al., 1997. Decay characteristics of HIV-1-infected compartments during combination therapy. Nature 387, 188–191.

Perelson, A.S., Nelson, P.W., 1999. Mathematical analysis of HIV-1 dynamics in vivo. SIAM Rev. 41, 3–44.

Perelson, A.S., Neumann, A.U., Markowitz, M., et al., 1996. HIV-1 dynamics in vivo: Virion clearance rate, infected cell life-span, and viral generation time. Science 271, 1582–1586.

Perelson, A.S., Ribeiro, R.M., 2013. Modeling the within-host dynamics of HIV infection. BMC Biol. 11, 96.

Prague, M., Gerold, J.M., Balelli, I., et al., 2019. Viral rebound kinetics following single and combination immunotherapy for HIV/SIV. bioRxiv http://dx.doi.org/10.1101/700401.

Puy, A., Beneventano, P., Levin, S.A., et al., 2022. Models with higher effective dimensions tend to produce more uncertain estimates. Sci. Adv. 8 (42), eabn9450.

Ramratnam, B., Bonhoeffer, S., Binley, J., et al., 1999. Rapid production and clearance of HIV-1 and hepatitis C virus assessed by large volume plasma apheresis. Lancet 354, 1782–1785.

Ramratnam, B., Mittler, J.E., Zhang, L., et al., 2000. The decay of the latent reservoir of replication-competent HIV-1 is inversely correlated with the extent of residual viral replication during prolonged anti-retroviral therapy. Nature Med. 6, 82–85.

Reu, P., Khosravi, A., Bernard, S., et al., 2017. The lifespan and turnover of microglia in the human brain. Cell Rep. 20, 779–784.

Richman, D.D., Margolis, D.M., Delaney, M., et al., 2009. The challenge of finding a cure for HIV infection. Science 323, 1304–1307.

Rong, L., Perelson, A.S., 2009a. Asymmetric division of activated latently infected cells may explain the decay kinetics of the HIV-1 latent reservoir and intermittent viral blips. Math. Biosci. 217, 77–87.

Rong, L., Perelson, A.S., 2009b. Modeling HIV persistence, the latent reservoir, and viral blips. J. Theoret. Biol. 260, 308–331.

Rong, L., Perelson, A.S., 2009c. Modeling latently infected cell activation: viral and latent reservoir persistence, and viral blips in HIV-infected patients on potent therapy. PLoS Comput. Biol. 5 (10), e1000533.

Sáez-Cirión, A., Bacchus, C., Hocqueloux, L., et al., 2013. Post-treatment HIV-1 controllers with a long-term virological remission after the interruption of early initiated antiretroviral therapy ANRS VISCONTI study. PLoS Pathog. 9 (3), e1003211.

Seay, K., Church, C., Zheng, J., et al., 2015. In vivo activation of human NK cells by treatment with an interleukin-15 superagonist potently inhibits acute in vivo HIV-1 infection in humanized mice. J. Virol. 89 (12), 6264–6274.

Sharova, N., Swingler, C., Sharkey, M., et al., 2005. Macrophages archive HIV-1 virions for dissemination in trans. EMBO J. 24, 2481–2489.

Shi, X., 1974. Basic Knowledge and Technical Methods of Medical Animal Experiments. The Fourth Military Medical University.

Shirakawa, K., Chavez, L., Hakre, S., et al., 2013. Reactivation of latent HIV by histone deacetylase inhibitors. Trends Microbiol. 21 (6), 277–285.

Shytaj, I., Norelli, S., Chirullo, B., et al., 2012. A highly intensified ART regimen induces long-term viral suppression and restriction of the viral reservoir in a simian AIDS model. PLoS Pathog. 8 (6), e1002774.

Siliciano, J.D., Kajdas, J., Finzi, D., et al., 2003. Long-term follow-up studies confirm the stability of the latent reservoir for HIV-1 in resting CD4+ T cells. Nature Med. 9, 727–728.

Skelton, J.K., Ortega-Prieto, A.M., Dorner, M., 2018. A hitchhiker's guide to humanized mice: new pathways to studying viral infections. Immunology 154, 50–61.

Stevenson, M., Gendelman, H.E., 1994. Cellular and viral determinants that regulate HIV-1 infection in macrophages. J. Leukoc. Biol. 56, 278–288.

Vaidya, N., Rong, L., 2017. Modeling pharmacodynamics on HIV latent infection: choice of drugs is key to successful cure via early therapy. SIAM J. Appl. Math. 77, 1781–1804.

Wang, X., Mink, G., Lin, D., et al., 2017a. Influence of raltegravir intensification on viral load and 2-LTR dynamics in HIV patients on suppressive antiretroviral therapy. J. Theoret. Biol. 416, 16–27.

Wang, S., Rong, L., 2014. Stochastic population switch may explain the latent reservoir stability and intermittent viral blips in HIV patients on suppressive therapy. J. Theoret. Biol. 360, 137–148.

Wang, X., Rong, L., 2019. HIV low viral load persistence under treatment: Insights from a model of cell-to-cell viral transmission. Appl. Math. Lett. 94, 44–51.

Wang, X., Song, X., Tang, S., et al., 2016. Dynamics of an HIV model with multiple infection stages and treatment with different drug classes. Bull. Math. Biol. 78, 322–349.

Wang, S., Xu, F., Rong, L., 2017b. Bistability analysis of an HIV model with immune response. J. Biol. Syst. 25 (04), 677–695.

Wege, A.K., Melkus, M.W., Denton, P.W., et al., 2008. Functional and phenotypic characterization of the humanized BLT mouse model. Curr. Top. Microbiol. Immunol. 324, 149–165.

Wolfgang, S., Sarah, F., Myra, M., et al., 2013. Duration of HIV-1 viral suppression on cessation of antiretroviral therapy in primary infection correlates with time on therapy. PLoS One 8 (10), e78287.

Wong, J.K., Hezareh, M., Günthard, H.F., et al., 1997. Recovery of replication-competent HIV despite prolonged suppression of plasma viremia. Science 278, 1291–1295.

Wu, H., Zhu, H., Miao, H., et al., 2008. Parameter identifiability and estimation of HIV/AIDS dynamic models. Bull. Math. Biol. 70, 785–799.

Yan, C., Wang, W., 2019. Modeling HIV dynamics under combination therapy with inducers and antibodies. Bull. Math. Biol. 81 (7), 2625–2648.